Instabilities in the flux-line lattice of anisotropic superconductors

A. M. Thompson and M. A. Moore
Theory Group, Department of Physics, University of Manchester, Manchester, M13 9PL, United Kingdom
(Received 22 January 1996; revised manuscript received 24 September 1996)

The stability of the flux-line lattice has been investigated within anisotropic London theory. This is a full-scale investigation of instabilities in the ''chain'' state, the equilibrium lattice that is similar to the Abrikosov lattice at large fields but crosses over smoothly to a pinstripe structure at low fields. By calculating the normal modes of the elasticity matrix, it has been found the lattice is stable at large fields, but that instabilities occur as the field is reduced. The field at which these instabilities first arise, $b^*(\epsilon,\theta)$, depends on the anisotropy ϵ and the angle θ at which the lattice is tilted away from the c axis. These instabilities initially occur at wave vector $\mathbf{k}^*(\epsilon,\theta)$. The dependence of $\mathbf{k}^*$ on ϵ and θ is complicated, but the component of $\mathbf{k}^*$ along the average direction of the flux lines, k_z, is always finite. For rigid straight flux lines, the cutoff necessary for London theory has been ''derived'' from Landau-Ginzburg theory, where the shape of the vortex core is known. However, for investigating instability at finite k_z it is necessary to know the dependence of the cutoff on k_z, and we have used a cutoff suggested by Sudbø and Brandt. The instabilities only occur for values of the anisotropy ϵ appropriate to a material like BSCCO, and not for anisotropies more appropriate to YBCO. The lower critical field $H_{c_1}(\phi)$ is calculated as a function of the angle ϕ at which the applied field is tilted away from the crystal axis. The presence of kinks in $H_{c_1}(\phi)$ is seen to be related to instabilities in the equilibrium flux-line structure. [S0163-1829(97)07605-4]

I. INTRODUCTION

The existence of novel-flux line structures in high-temperature superconductors has led to intensive investigation of the mixed state of these materials. Unusual structures have been observed in Bitter pattern experiments on YBCO (Refs. 1 and 2) and BSCCO (Refs. 3 and 4) when the applied magnetic field was tilted away from the c axis. In YBCO, the ''chain'' state was observed[1,2] where the anisotropy of the material causes the usual repulsive flux-line interaction to become attractive within the tilt plane, the plane containing the magnetic field and the c axis. The chain state had been predicted within the framework of the London approximation.[5,6]. In some of the experiments[2] the chains of flux lines were seen embedded in an approximately triangular flux-line lattice, but it is believed the presence of the lattice was due to pinning of the flux lines. In BSCCO, similar structures of chains embedded in a lattice were also seen,[3,4] but the dependence of the flux-line spacings on the tilt angle and magnetic field were different from those in YBCO, implying these structures may be created by a different mechanism. Possible explanations for the flux-line structure seen in BSCCO have been proposed.[7,8] It was suggested there existed interpenetrating flux-line lattices, one orientated approximately parallel to the c axis while the other is orientated approximately parallel to the ab plane. Within the framework of the London approximation, it has been shown that provided the anisotropy is large enough there is more than one possible angle at which the flux lines initially enter the sample.[8]

The mixed state for isotropic superconductors is a periodic triangular array of straight flux lines.[9] In uniaxially anisotropic superconductors it was predicted[10,11] the flux lines would form a distorted triangular lattice, where the spacings between the flux lines depend on the strength of the magnetic field $\mathbf{B}$ and the anisotropy mass ratio M_z/M. A lattice similar to this distorted triangular lattice has been observed in YBCO at large fields using small angle neutron scattering.[12]

The stability of this distorted lattice against elastic deformations has been studied extensively within London theory. Sudbø and Brandt[13] showed that at large anisotropy $M_z/M \gg 1$ and small magnetic induction $b = B/H_{c_2} \ll 1$ the energy associated with a pure shearing mode of the flux lattice can become negative. The existence of a tilt-wave instability, $\mathbf{k}=(0,0,k_z)$, was demonstrated by Sardella and Moore[14] and confirmed by Nguyen and Sudbø,[15] who both employed the same cutoff procedure. The distorted triangular lattice is the lattice one would expect using the ideas of anisotropic scaling.[16] The lattice's basis vectors are proportional to $1/\sqrt{b}$ and depend in a simple manner on θ, κ, ϵ. Minimizing the free energy, Daemen *et al.*[17] showed that out of the set of centered rectangle lattice structures, one of which is the distorted triangular lattice, the true equilibrium lattice behaves quite differently. At large fields it is approximately the distorted triangular (Abrikosov) lattice, but there is a smooth crossover to the ''chain'' state at small fields. This state has one of the basis vectors independent of the field, with the other being inversely proportional to b.

In this paper we investigate the stability of this equilibrium lattice at a general wave vector $\mathbf{k}=(k_x,k_y,k_z)$. The existence of a zone center instability has been observed;[18] this is a full-scale investigation of elastic instabilities of this equilibrium lattice. The cutoff used is that proposed by Sudbø and Brandt,[13] which depends on k_z. The lattice is found to be stable at large fields. As the field is reduced, the field at which the instability first occurs $b^*(\epsilon,\theta)$ depends on the anisotropy ϵ, and the angle θ at which the lattice is tilted from the c axis. The magnitude of these fields $b = B/H_{c_2} \sim O(10^{-4})$ is approximately that used in the experiments where the unusual flux-line structures were seen. It is generally believed these instabilities are somehow related to the different flux-line structures seen in experiments, but we have as yet no good theoretical interpretation of the connection.

The attractive vortex interaction also forces the flux lines to initially enter a superconductor not as single flux lines but in chains. For very large anisotropy, there exists the possibility that these chains may first enter the sample at more than one direction. The precise details are complicated, see Sec. VI. However, they indicate that for YBCO the chain state is the stable low-field structure. This is not the case for BSCCO, where it is possible the low-field structure will be the coexistence of different chain state orientations.

The initial instabilities observed always have *finite* k_z. For instabilities of nonzero k_z the form of the cutoff used within the London theory is crucial. In the calculation of Nguyen and Sudbø,[15] who used a cutoff that did not depend on k_z, the coexistence of different flux-line orientations and the zero-field tilt-wave instability were two different effects, i.e., they initially occurred at different anisotropies. In the limit $b \to 0$ it can be shown that the onset of both effects are related to the line tension $P_l(\theta)=\varepsilon_l(\theta)+\partial^2\varepsilon_l/\partial\theta^2$ becoming negative. If the cutoff that depends on k_z is used, it is found that the two effects do occur at the same anisotropy, implying this cutoff may be more reliable.

II. LONDON THEORY

A convenient way to describe the low-field magnetic properties of high-T_c superconductors is London theory. In the isotropic form, this theory just depends on the penetration depth λ and on $\kappa=\lambda/\xi$, where ξ is the coherence length. To allow for the anisotropy of the HTSC compounds, the square penetration depth λ^2 is replaced by the tensor $\lambda_{ij}^2=\Lambda_{ij}$. Here, we shall only investigate uniaxial anisotropy where $\Lambda_{XX}=\Lambda_{YY}=\lambda_{ab}^2\neq\Lambda_{ZZ}=\lambda_c^2$ are the only nonzero elements of Λ_{ij}. The anisotropy of the material is governed by the parameter ϵ which in the effective mass model is given by $\epsilon^2=M_X/M_Z$ and $\lambda_{ab}/\lambda_c=\xi_c/\xi_{ab}=\epsilon$.

The London free energy can be written as

$$F=\frac{1}{8\pi}\int d^3r\left\{\mathbf{H}^2+\left(\frac{\Phi_0}{2\pi}\nabla\varphi-\mathbf{A}\right)\mathbf{\Lambda}^{-1}\left(\frac{\Phi_0}{2\pi}\nabla\varphi-\mathbf{A}\right)\right\}, \tag{1}$$

where $\mathbf{A}$ is the vector potential of the magnetic field $\mathbf{H}=\nabla\times\mathbf{A}$, φ is the phase of the order parameter, Φ_0 is the flux quantum, and $\mathbf{\Lambda}^{-1}$ is the inverse of the square penetration depth tensor $\mathbf{\Lambda}$. The magnetic induction $\mathbf{B}$ is the average magnetic field $\mathbf{B}=\langle\mathbf{H}\rangle=B\hat{\mathbf{z}}$. London theory is a good approximation at low induction, $B<0.2H_{c_2}$,[19] where the cores do not overlap strongly.

In general, the $\mathbf{B}$ field is not aligned with the crystal axis, and we chose our coordinate system such that the $\mathbf{B}$ field lies in the X-Z plane and is tilted away from the c axis by an angle θ. It is then convenient to use the "vortex" coordinate system (xyz). This is obtained by rotating the crystal frame (XYZ) by an angle θ around the Y axis, see Fig. 1. In the vortex coordinate system, the square penetration depth is given by $\Lambda_{\alpha\beta}=\Lambda_1\delta_{\alpha\beta}+\Lambda_2 c_\alpha c_\beta$ where $\Lambda_1=\lambda_{ab}^2$, $\Lambda_2=\lambda_c^2-\lambda_{ab}^2$, $(\alpha,\beta)=(x,y,z)$, and c_α is the α component of the unit vector $\hat{\mathbf{c}}$ in the vortex frame.

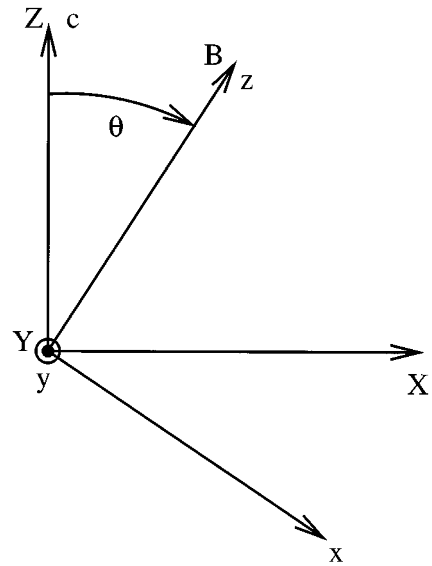

FIG. 1. The "vortex" frame (x,y,z) is obtained by rotating the crystal frame (X,Y,Z) by an angle θ about the Y axis.

The free energy (1) can be written in a simpler form. Minimizing Eq. (1) with respect to the vector potential $\mathbf{A}$, and then taking the curl of the equation, we obtain the London equation

$$\mathbf{H}+\nabla\times\{\mathbf{\Lambda}\cdot\nabla\times\mathbf{H}\}=\Phi_0\sum_i\int d\mathbf{r}_i\,\delta_3(\mathbf{r}-\mathbf{r}_i). \tag{2}$$

It is possible to derive this equation from the Ginzburg-Landau equations, assuming the order parameter has constant magnitude. The right-hand side of the London equation comes from $\nabla\times\nabla\varphi=\Sigma_i\int d\mathbf{r}_i\,\delta_3(\mathbf{r}-\mathbf{r}_i)$, where $\mathbf{r}_i$ is the position of the ith flux line.

The London equation is linear, and has the solution

$$\mathbf{H}_\alpha(\mathbf{r})=\Phi_0\sum_i\int d\mathbf{r}_i V_{\alpha\beta}(\mathbf{r}-\mathbf{r}_i). \tag{3}$$

Using this potential, the London free energy (1) may now be written as

$$F=\frac{\Phi_0^2}{8\pi}\sum_{i,j}\int\int d\mathbf{r}_i^\alpha d\mathbf{r}_j^\beta V_{\alpha\beta}(\mathbf{r}_i-\mathbf{r}_j). \tag{4}$$

The convention of summation over repeated indices is assumed. Written in this form, the free energy can be seen as consisting of two parts, the self-energy terms $(i=j)$ and the interaction terms $(i\neq j)$.

The Fourier transform of the potential $V(\mathbf{r}-\mathbf{r}_i)$ is [20]

$$V_{\alpha\beta}(\mathbf{k})=\frac{1}{1+\Lambda_1k^2}\left[\delta_{\alpha\beta}-\frac{\Lambda_2q_\alpha q_\beta}{1+\Lambda_1k^2+\Lambda_2q^2}\right], \tag{5}$$

where $\mathbf{q}=\mathbf{k}\times\hat{\mathbf{c}}$. From Eq. (5), we see that the potential decays only as $1/k^2$ as $k\to\infty$, implying that $\mathbf{H}(\mathbf{r})$ is singular at $\mathbf{r}=\mathbf{r}_i$. The singularites in $\mathbf{H}(\mathbf{r})$ are due to the absence of the vortex cores from London theory. A convenient way to circumvent the problems associated with the divergences is to introduce a cutoff into the London potential (5) via

$$V_{\alpha\beta}(\mathbf{k})=\frac{S(\mathbf{k})}{1+\Lambda_1 k^2}\left[\delta_{\alpha\beta}-\frac{\Lambda_2 q_\alpha q_\beta}{1+\Lambda_1 k^2+\Lambda_2 q^2}\right]. \qquad (6)$$

This is equivalent to replacing the δ function in the London equation (2) with a short-ranged function $S(\mathbf{r}-\mathbf{r}_i)$. By making this short-ranged function a Gaussian, of width $\sqrt{2}\xi_{ab}$ along a and b and width $\sqrt{2}\xi_c$ along c, the cutoff becomes[13,21]

$$S(\mathbf{k})=\exp-2g(\mathbf{k}),$$

$$g(\mathbf{k})=\xi_{ab}^2(\mathbf{k}\times\mathbf{c})^2+\xi_c^2(\mathbf{k}\cdot\mathbf{c})^2 \qquad (7)$$

$$=\xi_{ab}^2 q^2+\xi_c^2(k^2-q^2).$$

This provides an elliptical cutoff at large $\mathbf{k}_\perp=(k_x,k_y)$, as required from the shape of the core in Ginzburg-Landau theory.[22] The factor 2 in the exponential of $S(\mathbf{k})$ is just convention, but it can be determined more accurately by comparison with results from Ginzburg-Landau theory. The results in this paper are not affected by the choice of this parameter.

The exact form of the cutoff is of some debate. For straight rigid vortices the form of the cutoff can be derived from the shape of the core within Ginzburg-Landau theory.[22] However, the cutoff in Eq. (7) depends on k_z, the component of $\mathbf{k}$ in direction of the $\mathbf{B}$ field. Sardella and Moore[14] and Nguyen and Sudbø[15] investigated the tilt-wave instabilities of the distorted triangular lattice using a cutoff that depended only on $\mathbf{k}_\perp=(k_x,k_y)$, i.e., $g(\mathbf{k})=g(\mathbf{k}_\perp)=\xi_{ab}^2(\mathbf{k}_\perp\times\mathbf{c})^2+\xi_c^2(\mathbf{k}_\perp\cdot\mathbf{c})^2$ in Eq. (7). We believe the cutoff in Eq. (7) is more physical, as it does not depend on being able to specify $\mathbf{k}_\perp$. That can only be done by reference to the average direction of the flux lines, i.e., $\mathbf{B}$, but it is hard to believe that the cutoff should be sensitive to this overall average direction. Some authors do not use a cutoff function $S(\mathbf{k})$, but instead introduce an upper limit on any integrations over $\mathbf{k}$. In most situations, if the symmetry of the upper limit introduced is the same as the cutoff function $S(\mathbf{k})$, then similar results are obtained.[15] However, in some situations care may be required to ensure it is does not matter whether certain points in $\mathbf{k}$ space are just inside or outside the integration range.[23]

III. EQUILIBRIUM LATTICE

In an isotropic superconductor, the equilibrium flux-line lattice is a periodic array where the unit cell is defined by an equilateral triangle. Defining the x axis to coincide with one of the basis vectors, the basis vectors may be written as $\mathbf{R}_1=a\hat{\mathbf{x}}$ and $\mathbf{R}_2=a(\hat{\mathbf{x}}+\sqrt{3}\hat{\mathbf{y}})/2$ where $a^2=2\Phi_0/\sqrt{3}B$. The presence of anisotropy causes the lattice to distort from this equilateral structure. Using the ideas of anisotropic rescaling,[16] the lattice is expected to be of the form

$$\mathbf{R}_1=a\gamma\hat{\mathbf{x}},$$

$$\mathbf{R}_2=a(\gamma\hat{\mathbf{x}}+\sqrt{3}\hat{\mathbf{y}}/\gamma)/2, \qquad (8)$$

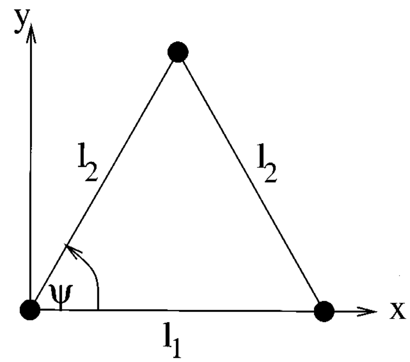

FIG. 2. The unit cell of a ‘‘chain’’ state.

where $\gamma^4=\cos^2\theta+\epsilon^2\sin^2\theta$. This structure is indeed the equilibrium structure in the limit of the lowest Landau level, and was seen to minimize the free energy of a set of rescaled structures.[24] All the length scales depend on the strength of the magnetic field in a similar manner, i.e., they are proportional to $1/\sqrt{b}$. We refer to this rescaled structure as the Abrikosov lattice.

The presence of anisotropy dramatically changes the profile of the magnetic field. If the anisotropy is large, the magnetic field associated with a single isolated flux-line contains regions around the flux-line where the local magnetic field points in the opposite direction to the average field. This allows the usually repulsive flux-line interaction to be attractive.

Daemen *et al.*[17] showed if we investigate the set of flux-line structures with a centered rectangular symmetry, one of which will be the same structure as the Abrikosov lattice, different equilibrium structures can be seen. The unit cell consists of an isosceles triangle, see Fig. 2, with two sides of length l_2 the other length l_1, with an angle ψ between sides of length l_1 and l_2. The lattice vectors are

$$\mathbf{R}_{mn}=(ml_1+nl_2\cos\psi)\hat{\mathbf{x}}+nl_2\sin\psi\hat{\mathbf{y}}, \qquad (9)$$

where m and n are integers. Repeated computer minimizations of the total free energy have confirmed that for uniaxial anisotropy the assumption the unit cell is an isosceles triangle is valid.[17] The magnetic flux per unit cell must be one flux quantum, which allows l_1, l_2 and ψ to be written in terms of one parameter

$$l_1=\sqrt{\frac{\Phi_0}{B}\frac{\rho}{\{1-[(1/2)\rho]^2\}^{1/2}}},$$

$$l_2=l_1/\rho, \qquad (10)$$

$$\cos\psi=\frac{1}{2}\rho.$$

Following Daemen *et al.*[17] we minimize the free energy per unit cell ε using the golden-section-search method[25] because the derivatives of ε with respect to ρ are hard to calculate.

The dependence of l_1 and l_2 on the field, $b=B/H_{c_2}(\theta=0)$, is shown in Fig. 3. At large fields the two lengths scale as approximately $1/\sqrt{b}$ but there is a smooth crossover to a regime at lower fields where one is approximately constant while the other scales as $1/b$. The region

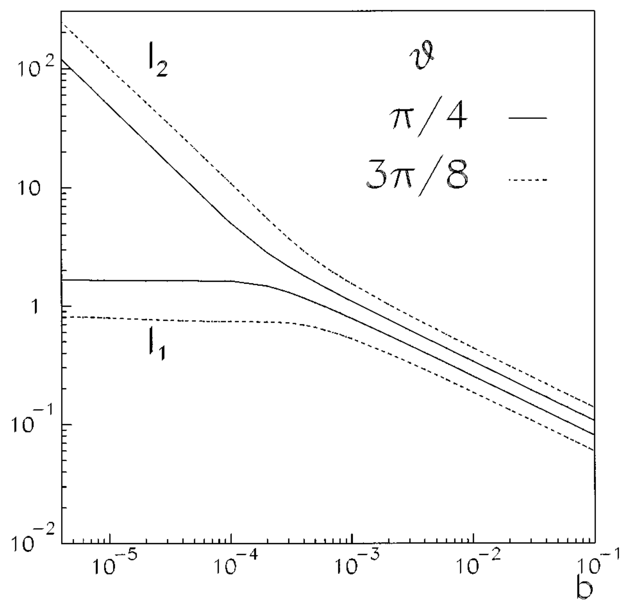

FIG. 3. The field dependence of the separation of the flux lines (measured in λ_{ab}) for $\epsilon = 1/60$ and $\kappa = 50$. At large fields l_1 and l_2 are proportional to $1/\sqrt{b}$ but at lower fields there is a crossover to the ''chain'' state.

where this crossover occurs is characterized by κ, θ, and ϵ. The low-field equilibrium state corresponds to the chain state, or ''pinstripe structure'' observed by Gammel *et al.*[1] in YBCO. This shows care must be taken in defining the flux line lattice in any calculation, as in this low-field regime the Abrikosov state is not an equilibrium state, see Fig. 4. The

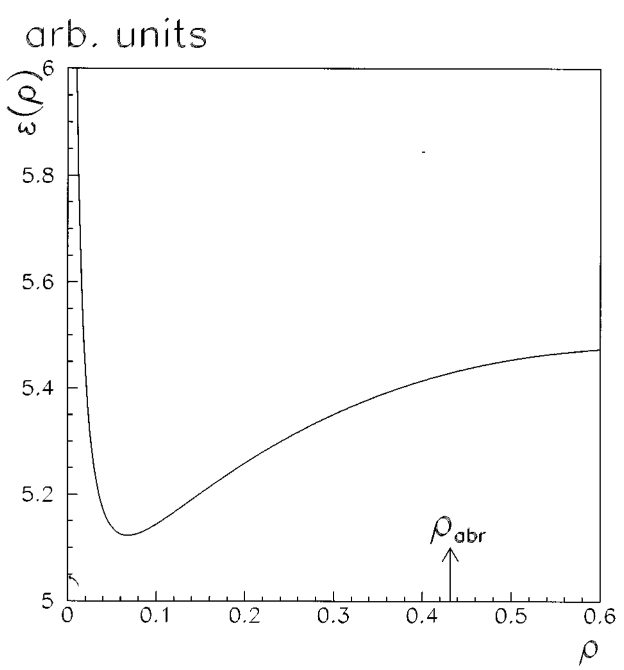

FIG. 4. The dependence of the energy per flux line on the parameter ρ, for $\epsilon = 1/60$, $\theta = 3\pi/8$, $\kappa = 50$, $b = 10^{-4}$. The arrow marks the value of ρ of the rescaled Abrikosov lattice. This figure clearly shows that the Abrikosov lattice is not the solution of minimum free energy.

value of ρ corresponding to the anisotropically rescaled Abrikosov lattice is given by ρ_{Abr}.

The reciprocal lattice of this equilibrium lattice has basis vectors

$$\mathbf{Q}_{mn} = n\frac{2\pi}{l_1}\hat{\mathbf{x}} + \left[m\frac{2\pi}{l_2} - n\frac{2\pi}{l_1}\cos\psi \right]\frac{1}{\sin\psi}\hat{\mathbf{y}}. \tag{11}$$

In the calculations that follow, wave vectors will be measured in units of $[2\pi/(3l_1)\hat{\mathbf{x}}, \pi/(l_2\sin\psi)\hat{\mathbf{y}}]$, making the rescaled reciprocal lattice vectors $\widetilde{\mathbf{Q}}_{mn} = 3n\hat{\mathbf{x}} + (2m-n)\hat{\mathbf{y}}$.

IV. ELASTIC THEORY OF FLUX-LINE LATTICE

The minimum free energy configuration of the flux lines has been assumed to be a periodic array, whose unit cell is an isosceles triangle with the base orientated along the x axis. To check the assumption that this free energy is at least a local minimum, the change in the free energy associated with small displacements $s_\alpha[\mathbf{R}_i(z)]$, $\alpha = (x,y)$, from the equilibrium lattice $\mathbf{R}_i = n\mathbf{R}_1 + m\mathbf{R}_2$ can be derived.[26,27] Keeping terms only to second order in the displacements $s_\alpha(\mathbf{R}_i)$ the change in the free energy is

$$\Delta F = \frac{1}{2}\int d^3\mathbf{k}\, s_\alpha(-\mathbf{k})\Phi_{\alpha\beta}(\mathbf{k})s_\beta(\mathbf{k}), \tag{12}$$

where the integration over $\mathbf{k}_\perp = (k_x, k_y)$ runs over the first Brillouin zone and over k_z on the interval $(-\infty, \infty)$. The elasticity matrix is

$$\Phi_{\alpha\beta}(\mathbf{k}) = \frac{B^2}{4\pi}\sum_{\mathbf{Q}} \{f_{\alpha\beta}(\mathbf{k}+\mathbf{Q}) - f_{\alpha\beta}(\mathbf{Q})\}, \tag{13}$$

where

$$f_{\alpha\beta}(\mathbf{p}) = p_z^2 V_{\alpha\beta}(\mathbf{p}) + p_\alpha p_\beta V_{zz}(\mathbf{p}) - p_z p_\alpha V_{z\beta}(\mathbf{p}) - p_z p_\beta V_{z\alpha}(\mathbf{p}). \tag{14}$$

The stability of a periodic lattice may be determined by investigating whether the normal modes of the elasticity matrix $\Phi_{\alpha\beta}(\mathbf{k})$ always remain stable, i.e., the eigenvalues of $\Phi_{\alpha\beta}(\mathbf{k})$ are positive, or whether in some regions of the Brillouin zone the normal modes become unstable.

The stability of the distorted triangular lattice (Abrikosov lattice) has been examined by various authors. [13–15] Sudbø and Brandt[13] observed that for a configuration of rigid flux lines, i.e., $k_z = 0$, as the magnetic field was reduced below a specific level the normal modes became unstable. Sardella and Moore[14] observed a tilt-wave instability, $k_x = k_y = 0$, $k_z \neq 0$, and this instability was present in all fields. However, the cutoff used did not depend on k_z. It was suggested that with the use of the cutoff of Eq. (7) the instability would disappear.[21] For $\mathbf{k} = (0,0,k_z)$ the elasticity matrix is diagonal, and the instability calculated by Sardella and Moore was associated with Φ_{yy} becoming negative. Upon repeating the calculation of Sardella and Moore with the cutoff (7), we found that the eigenvalue Φ_{yy} did indeed remain positive. However, Φ_{xx} became more unstable, and as in Ref. 13, the lattice becomes unstable as the field is reduced beyond a

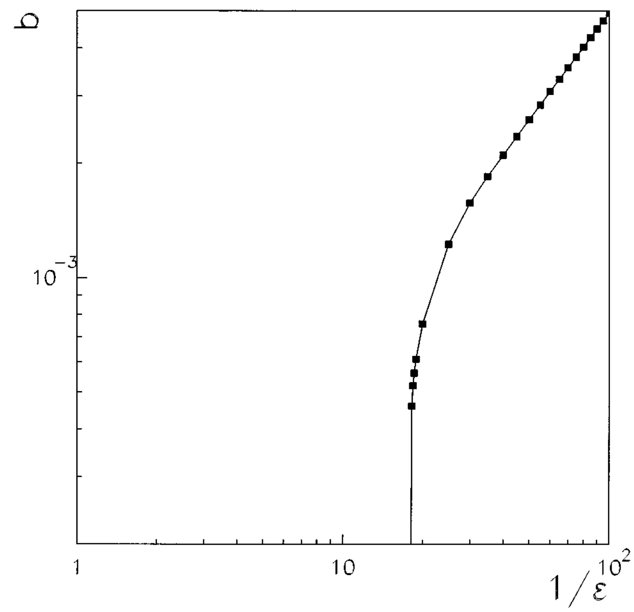

FIG. 5. The field at which the lattice initially becomes unstable as a function of the anisotropy ϵ, for $\theta=3\pi/8$ and $\kappa=50$.

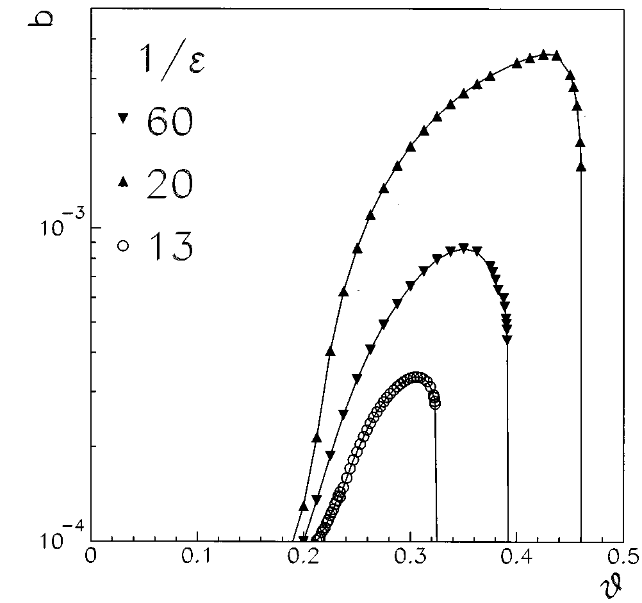

FIG. 6. The field at which the lattice initially becomes unstable as a function of the angle, θ, by which the lattice is tilted from the c axis, for different values of ϵ and $\kappa=50$.

critical level. Nguyen and Sudbø[15] have confirmed this by calculating the normal modes of rigid flux lines in the limit $b=0$.

The Abrikosov lattice is only a good approximation of the equilibrium structure at fields $b>O(10^{-2}-10^{-3})$. We have investigated the normal modes of the elasticity matrix $\Phi_{\alpha\beta}(\mathbf{k})$ for $\mathbf{k}=(k_x,k_y,k_z)$, with the equilibrium lattice being the isosceles triangle described in Sec. III, using the k_z dependent cutoff (7). The presence of instabilities is expected as Sardella[18] has confirmed the existence of a zone center instability for large tilt angles θ, large anisotropy $1/\epsilon$ and small fields b.

The fields at which instabilities are observed depend on κ, on the tilt angle θ and on the anisotropy ϵ. The isotropic system, $\epsilon=1$, is stable. As the anisotropy increases, ϵ decreases, no instabilities are observed until a critical anisotropy is obtained. The minimum anisotropy required for instabilities to be seen depends on κ. For $\kappa=20$ instabilities were seen for $1/\epsilon^2>120.3$, but this was increased to $1/\epsilon^2>138$ for $\kappa=50$. For values of $1/\epsilon$ less than these critical values the lattice is stable at *all* orientations.

If the anisotropy is larger than this critical anisotropy, instabilities can be seen. The lattice is always stable at large fields. As the field is reduced there is a specific field $b^*(\kappa,\epsilon,\theta)$ at which the lattice *initially* becomes unstable. Figure 5 shows that for a given angle θ there is a minimum anisotropy $1/\epsilon$ below which the lattice is stable in all fields. It also shows that the critical field b^* increases as the system becomes more anisotropic. The lattice is always stable at $\theta=0$ and $\theta=\pi/2$, but once the anisotropy is large enough there exists a range of angles at which instabilities are seen, see Fig. 6. This range of angle increases as the anisotropy increases.

The wave vectors at which these instabilities are first seen, $\mathbf{k}^*(\kappa,\epsilon,\theta)$ always have *finite* k_z. Both b^* and $\mathbf{k}^*$ are functions of κ, ϵ, and θ. These unstable modes correspond to displacements of the lattice approximately parallel to the x axis, and we call it the ''staircase wave'' instability to distinguish it from other instabilities observed. In Fig. 7 the dependence of the x and y components of k^* are shown; k_x and k_y have been rescaled so that the dashed line shows the edge of the first Brillouin zone. θ decreases from small k_x to large k_x. The explanation of the behavior of the actual wave vector where the instability first appears, $\mathbf{k}^*$, is not obvious to us.

The parameters chosen in this paper ($\epsilon=1/60$, $\kappa=50$) were chosen to give some insight into the behavior of BSCCO. While the exact value of the anisotropy in BSCCO

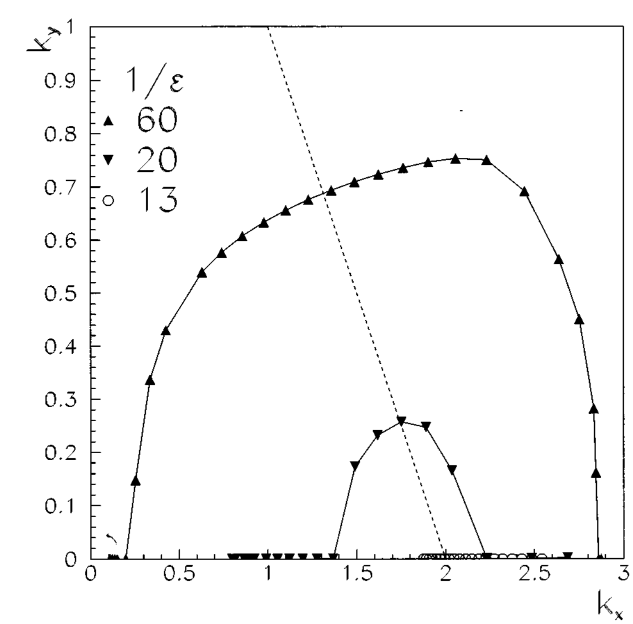

FIG. 7. The rescaled k_x and k_y components of $\mathbf{k}^*$, for different ϵ and $\kappa=50$. The dashed line marks the edge of the first Brillouin zone.

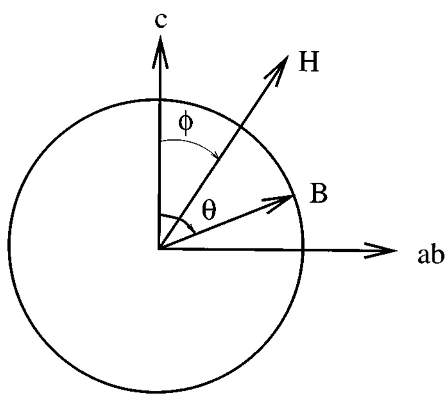

FIG. 8. The geometry of sample and applied field $\mathcal{H}$. The applied field is tilted at an angle ϕ from the c axis, while the magnetic induction **B** is tilted at an angle θ.

is unknown, the values used in this paper are similar to those used in other papers.[13–15] In comparison, YBCO is much less anisotropic, with $\epsilon\approx 1/5$ and $\kappa\approx 50$, and as can be seen from Fig. 5 is well below that required for the instabilities to be observed. To explore the instabilities in full detail as a function of κ, ϵ, θ, and b is very time consuming, but Fig. 5 shows the ''chain'' state is stable for parameters that could describe YBCO, but unstable for BSCCO.

V. LOWER CRITICAL FIELD: ABRIKOSOV LATTICE LIMIT

The presence of elastic instabilities for very anisotropic materials may indicate why there are differences in the Bitter patterns observed for BSCCO and YBCO. One interpretation of the BSCCO patterns was the coexistence of two interpenetrating lattices.[7,8] This postulate has been investigated by calculating the angles at which single flux lines first enter a superconducting sample.[13,15] We modify the calculation of Nguyen and Sudbø[15] to show this possible effect in order to emphasize the importance of the cutoff procedure used.

We consider a cylindrical superconducting sample, with the applied field $\mathcal{H}$ perpendicular to the axis of the cylinder, and tilted at an angle ϕ away from the crystal c axis, see Fig. 8. This geometry is chosen so that demagnetization effects permit solutions where the flux lines are straight for all orientations of the applied field.

Within this geometry, the Gibbs free energy for a system of rigid straight flux lines, tilted at (a different) angle θ is

$$G=F-\frac{B\mathcal{H}\cos(\phi-\theta)}{4\pi}. \tag{15}$$

Neglecting the interaction between the flux lines, the free energy within the London approximation (4) is

$$F=\frac{B^2}{8\pi}\int\frac{d^2\mathbf{q}}{4\pi^2}S(\mathbf{q})\frac{1+\lambda_\theta^2q^2}{(1+\lambda_{ab}^2q^2)(1+\lambda_\theta^2q_x^2+\lambda_c^2q_y^2)}, \tag{16}$$

where $\lambda_\theta^2=\lambda_{ab}^2\sin^2\theta+\lambda_c^2\cos^2\theta$. As with most calculations within the London approximation, the integral is formally divergent without the cutoff term, but the use of the cutoff $S(\mathbf{q})$ described in the previous section allows the calculation to proceed. Also, as the integration is over $\mathbf{q}$ perpendicular to the flux line this calculation is insensitive to the q_z dependence of the cutoff $S(\mathbf{q})$. By neglecting the interaction between the flux lines we are essentially just discussing the behavior of a single flux line. This calculation can be viewed as the extension of the Abrikosov lattice to $b=0$.

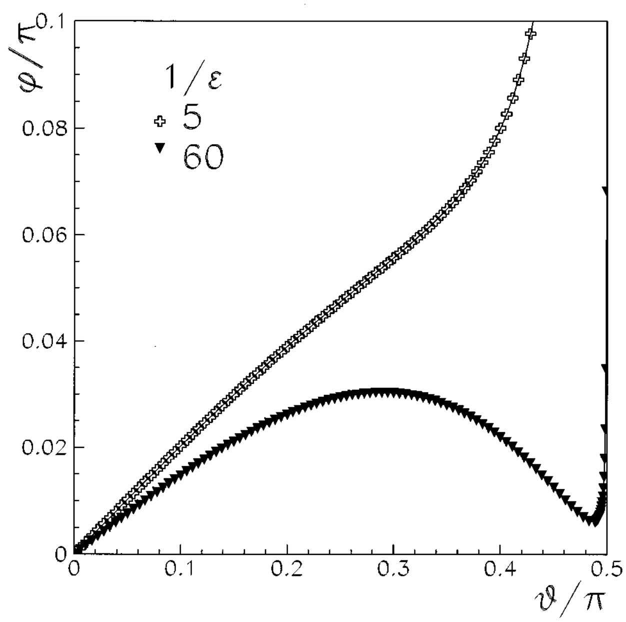

FIG. 9. The relationship between θ and ϕ for different anisotropies, with $\kappa=50$. This relationship becomes nonmonotonic over a range of angles for large anisotropy.

As the field $\mathcal{H}$ is increased, the flux lines initially enter the sample when $G=0$. Although it would be preferable to chose ϕ, the orientation of the applied field, and then calculate θ and $\mathcal{H}$ it is only possible to assume θ and then calculate the corresponding values of $\mathcal{H}$ and ϕ. Looking for solutions where $\partial G/\partial\theta=0$ implies the orientation(s) of the flux lines within the sample are governed by the relation

$$\tan\phi=\frac{\tan\theta+F'/F}{1-F'\tan\theta/F}. \tag{17}$$

When investigating the first entry of flux lines into the sample, it is well known that the cutoff used is important. If a circular cutoff is used then there is a unique orientation of the flux lines, given by[8,15]

$$\tan\phi=\epsilon^2\tan\theta. \tag{18}$$

However, this is not true if an elliptical cutoff is used, as for large anisotropies there exists a nonmonotonic relation between θ and ϕ, see Fig. 9. This implies the possibility of the existence of two orientations of flux lines.

Within the nonmonotonic regime, there exist three possible orientations of the flux lines, θ_a, θ_b, and θ_c, for any given ϕ. θ_b corresponds to an unstable orientation of the flux lines, i.e., a maximum in the Gibbs free energy, and will not be considered further.

By calculating the Gibbs free energy, we can see whether the flux lines will orientate at either θ_a or θ_c, and the relationship between ϕ and θ determined. A ''forbidden'' region

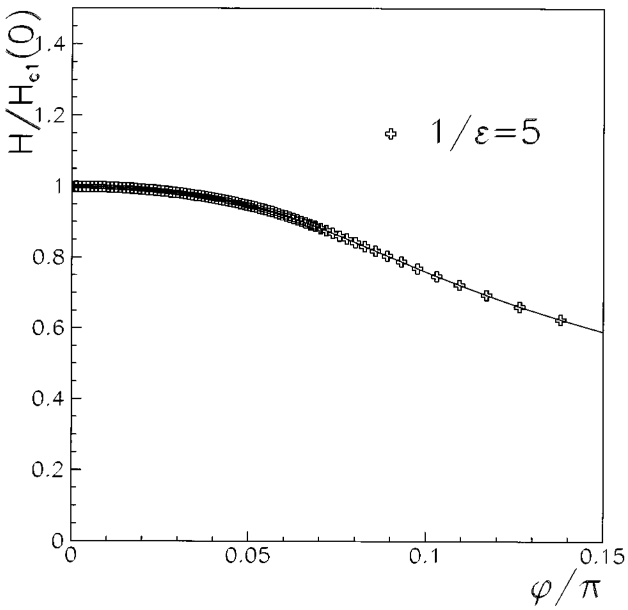

FIG. 10. The applied field $\mathcal{H}(\phi)$ for $\epsilon=1/5$ and $\kappa=50$.

occurs due to the presence of the nonmonotonic regime. The flux-line lattice can only be orientated at angles $\theta<\theta_1^*$ and $\theta>\theta_2^*$.

This can be seen by noting the relationship between the calculated values of $\mathcal{H}$ and ϕ. Figure 10 shows $\mathcal{H}(\phi)$ when all flux-line orientations are allowed. The points in Fig. 10 are equally spaced in θ. For large anisotropy $\mathcal{H}(\phi)$ becomes nonmonotonic when $\theta(\phi)$ becomes nonmonotonic. In Fig. 11 the three values of $\mathcal{H}(\phi)$ in the nonmonotonic regime correspond to the three possible orientations of the flux lines at θ_a, θ_b, and θ_c. While all three orientations correspond to $G=0$ and $\partial G/\partial\theta=0$, only one is a global minimum in $G(\theta)$. This global minimum will be the equilibrium structure and is the orientation with the smallest value of $\mathcal{H}(\phi)$. The lower critical field $H_{c_1}(\phi)$ is therefore just the smallest value of $\mathcal{H}(\phi)$ for any given ϕ. From Fig. 11 it can be seen H_{c_1} has a kink where $\mathcal{H}(\theta_1^*)=\mathcal{H}(\theta_2^*)$ and $\phi(\theta_1^*)=\phi(\theta_2^*)=\phi_{\text{kink}}$. The presence of kinks in the lower critical field for single flux lines have also been observed within the Ginzburg-Landau model.[22]

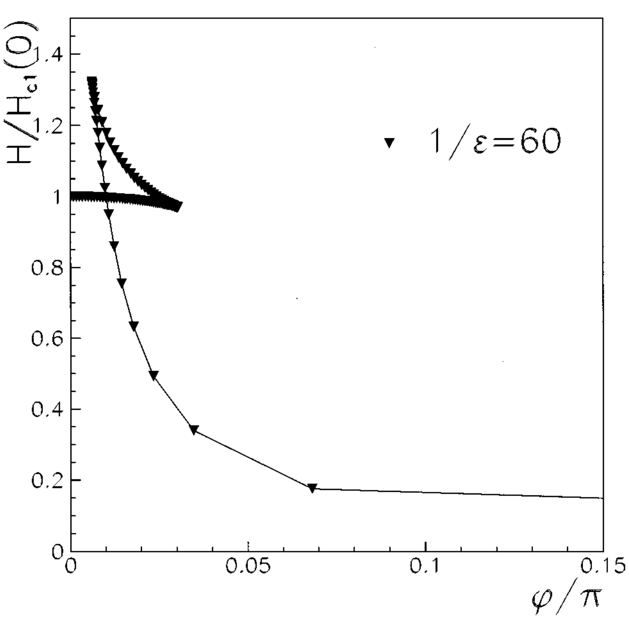

FIG. 11. The applied field $\mathcal{H}(\phi)$ for $\epsilon=1/60$ and $\kappa=50$.

If we now allow the superposition of noninteracting flux lines, which are assumed to be far apart in the limit $b\to 0$, the ''forbidden region'' may be removed. At $H_{c_1}(\phi_{\text{kink}})$ the average field $\mathbf{B}$ may be orientated at all angles within the ''forbidden'' region $\theta_1^*<\theta<\theta_2^*$ by orientating some flux lines at θ_1^* and the others at θ_2^*.

Various authors have discussed the competition between the coexistence of different flux-line species and the presence of elastic instabilities in the supposed equilibrium structure. For single isolated flux lines (in the limit $b\to 0$) the elastic instabilities depend most strongly on k_z and only tilt-wave instabilities will be discussed further in this section.

As k_z is nonzero, the cutoff used is important. Nguyen and Sudbø used $S(\mathbf{k})=S(\mathbf{k}_\perp)$. For any given value of κ they found two important values of the anisotropy. At small anisotropies the relationship between ϕ and θ is monotonic. For $1/\epsilon>\Gamma_1^{\text{NS}}$ the relationship between ϕ and θ becomes nonmonotonic and the Gibbs free energy may be doubly degenerate. However, if $1/\epsilon>\Gamma_2^{\text{NS}}$ the ''perpendicular'' tilt modulus $c_{44}^\perp(\mathbf{k})=\Phi_{xx}(0,0,k_z)/k_z^2$ becomes negative over a range of angles. The two critical anisotropies depend linearly on $\ln\kappa$, but Γ_2^{NS} is much larger than Γ_1^{NS}.

There is a marked difference if the cutoff $S(\mathbf{k})=\exp[-2g(\mathbf{k})]$, $g(\mathbf{k})=\xi_{ab}^2(\mathbf{k}\times\mathbf{c})^2+\xi_c^2(\mathbf{k}\cdot\mathbf{c})^2$. The dependence of Γ_1^{NS} and Γ_2^{NS} on κ is similar, but $\Gamma_1^{\text{NS}}=\Gamma_2^{\text{NS}}=\Gamma$. For $\kappa=50$ and $S(\mathbf{k})=\exp[-2g(\mathbf{k})]$ it is found $\Gamma\approx 9.65$. The value of Γ does depend on the cutoff procedure used. Using a cutoff of the same symmetry but a different strength, $S(\mathbf{k})=\exp[-g(\mathbf{k})]$, it is found $\Gamma\approx 10.03$ for $\kappa=50$.

These two ''competing'' effects are both related to the line tension $P_l(\theta)=\varepsilon_l(\theta)+\partial^2\varepsilon_l(\theta)/\partial\theta^2$, where ε is the line energy. In the limit $b\to 0$ where the London free energy $F=n\varepsilon_l$, n is the areal density of flux lines, then it follows from Eq. (17) that

$$P_l(\theta)=\varepsilon_l(\theta)\sec^2(\phi-\theta)\frac{\partial\phi}{\partial\theta}. \tag{19}$$

However, c_{44} may be defined as $c_{44}=d^2F(\theta)/d\theta^2$. For the isolated noninteracting flux-lines $F=n\varepsilon_l$, so $c_{44}\propto\varepsilon_l(\theta)+\partial^2\varepsilon_l(\theta)/\partial\theta^2=P_l(\theta)$,[28] where the first term is due to the compression of the flux-line lattice during tilting. Therefore the presence of a kink in $H_{c_1}(\phi)$ not only causes a restriction of orientations of the flux-line lattice, and the possibility of the coexistence of different flux-line orientations, but is also related to the presence of a tilt-wave instability. The tilt-wave instabilities only occur where $\partial\phi/\partial\theta<0$, see also Grishin *et al.*,[5] but this is only part of the region of excluded flux line orientations $\theta_1^*<\theta<\theta_2^*$ and the instabilities are never observed.

VI. LOWER CRITICAL FIELD: CHAIN STATE LIMIT

The previous calculation assumed the equilibrium low-field flux-line structure was a configuration of well-separated noninteracting flux lines, i.e., the extension of the Abrikosov lattice to $b=0$. In Sec. III it was seen the low-field equilibrium structures are very different from the Abrikosov lattice. The anisotropy induced attractive interaction makes it easier for chains of flux lines to enter a sample than for single flux lines, which forces H_{c_1} for an single infinite chain to be less than H_{c_1} for a single flux line.[5] We take the limit $b \to 0$ to imply there is only one vortex chain in the sample, the separation between the chains being effectively infinite.

The presence of instabilities in the ''chain'' state were investigated in Sec. IV, which seemed to indicate a different behavior for materials such as YBCO from those such as BSCCO. These instabilities were seen as the field was reduced from a stable regime similar to the Abrikosov lattice. In this section we investigate what happens as the flux lines initially enter the sample, i.e., $b=0$. Chosing the same geometry as Sec. V we again look at the relationship between ϕ and θ and relate this to the elastic instabilities.

For a single flux line in section V, the 2D line energy integral is easily calculated by rescaling the coordinates, see Nguyen and Sudbø.[15] For the single infinite chain, this 2D integral is replaced by a sum over the reciprocal lattice vectors of the 1D chain and a 1D integral perpendicular to the chain. Assuming the chain to be a set of flux lines equally spaced along the x axis, then

$$\int \frac{d^2\mathbf{q}}{(2\pi)^2} \to \frac{1}{l_{\rm ch}} \sum_n \int \frac{dq_y}{2\pi}, \tag{20}$$

where $q_x = 2\pi n / l_{\rm ch}$, $n = 0 \pm 1 \pm 2 \ldots$, $l_{\rm ch}$ being the separation of the flux lines in the chain. $l_{\rm ch}$ is determined by finding the minimum in the line energy, and is a nonmonotonic function of θ.

The behavior of the chain state is subtly different from that of the single flux line. The main effects are the same, i.e., for large anisotropy there exist a range of angles over which the chains cannot be orientated, but the details are more complicated.

The chain state is stable for small anisotropies, but for large anisotropies the relationship between ϕ and θ once again becomes nonmonotonic. For this to occur it requires a larger anisotropy than for the single flux line. Figure 12 shows $\phi(\theta)$ just after the onset of nonmonotonicity for isolated flux lines. The chain state has no restriction on the orientation of the flux lines, unlike the single flux line, and also the chain state always has a lower (or equal) lower critical field H_{c_1},[5] see Fig. 13.

Increasing the anisotropy, Fig. 14, the chain state eventually shows signs of instabilities. Initially $\phi(\theta)$ becomes nonmonotonic at large tilt angles, $\theta \approx 9\pi/20$, and the chains are excluded over the range $\theta^*_{2'} < \theta < \theta^*_2$. This occurs for $1/\epsilon > \Gamma_1(\kappa)$ and $H_{c_1}(\phi)$ contains a kink in a manner similar to the single flux line.

However, for $1/\epsilon > \Gamma_2(\kappa)$, $\phi(\theta)$ is also nonmonotonic at smaller angles, $\theta \approx \pi/4$. This implies the chains are also excluded over a different range $\theta^*_1 < \theta < \theta^*_{1'}$. From $\mathcal{H}(\phi)$, Fig.

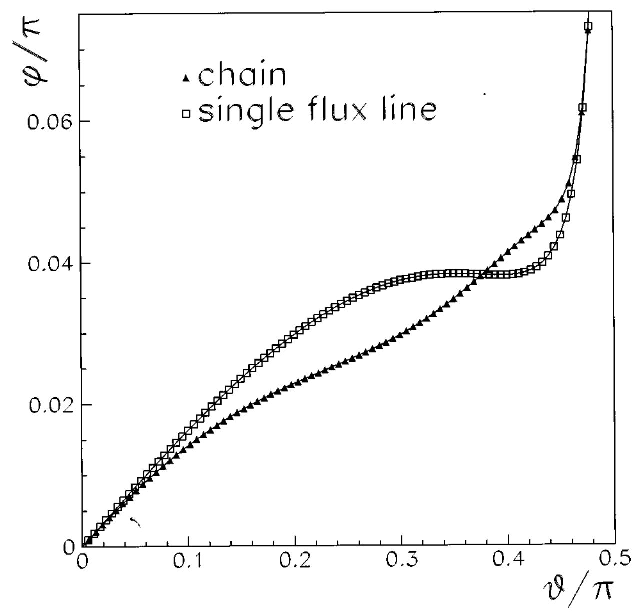

FIG. 12. The relationship between ϕ and θ for different lattices, with $\kappa=50$ and $\epsilon=1/10$.

15, it can be seen that a stable range $\theta^*_{1'} < \theta < \theta^*_{2'}$ exists between these two forbidden regions. The lower critical field $H_{c_1}(\phi)$ now has two kinks. As the anisotropy is increased further these excluded regions grow until at $1/\epsilon > \Gamma_3(\kappa)$ the chain state is excluded over the whole range $\theta^*_1 < \theta < \theta^*_2$. The second kink in $H_{c_1}(\phi)$ disappears, Fig. 16, and only one kink remains. For $\kappa=50$, $\Gamma_1 \approx 15$, $\Gamma_2 \approx 30$, and $\Gamma_3 \approx 60$.

The elastic instabilities again only occur when $\partial\phi/\partial\theta < 0$. These instabilities have slightly different properties at small θ and large θ. At large θ the lattice is most unstable to a tilt-wave instability $\mathbf{k}=(0,0,k_z)$ while it is a staircase wave instability, with k_x and k_z both nonzero, that

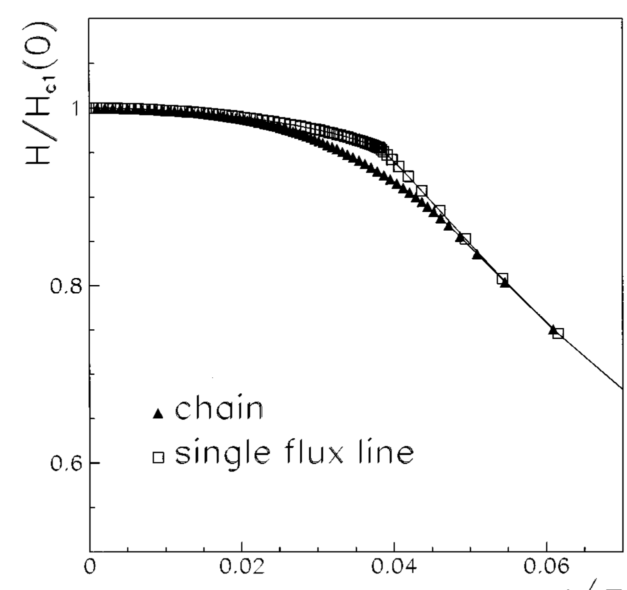

FIG. 13. The applied field $\mathcal{H}(\phi)$ for different lattices, with $\kappa=50$ and $\epsilon=1/10$.

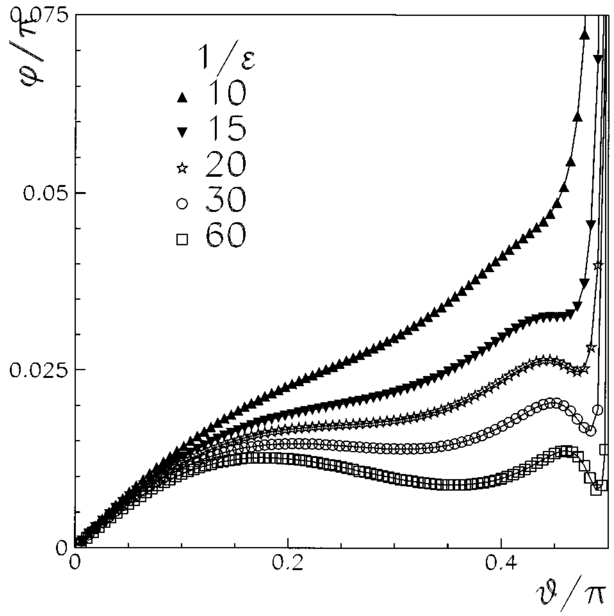

FIG. 14. The relationship between ϕ and θ for different anisotropies, with $\kappa=50$.

causes the chain to become unstable at smaller θ. Again, these instabilities only occur in the forbidden regions, and the chain state is stable at all allowed orientations.

VII. CONCLUSION

We have investigated the presence of instabilities in the flux-line lattice in anisotropic superconductors using London theory. There are limitations on the applicability of the London theory, but the wave vectors at which the instabilities appear are well within its limits of validity, i.e., $\mathbf{k} \ll O(1/\xi)$.

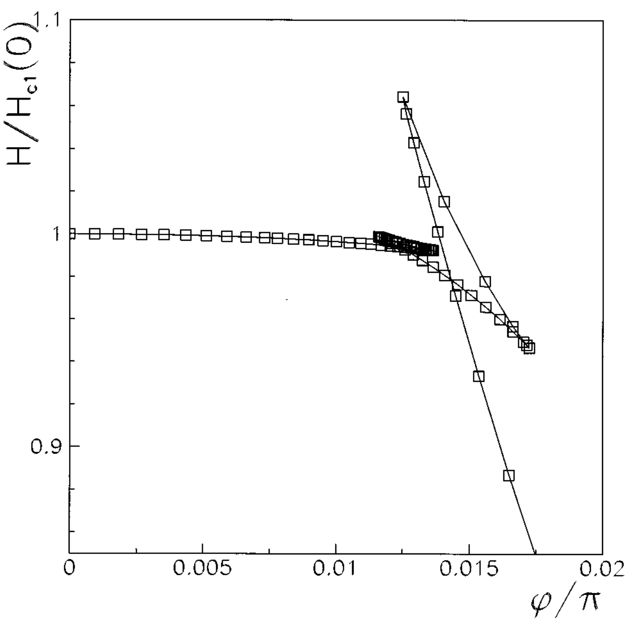

FIG. 15. The relationship between $\mathcal{H}$ and ϕ showing the existence of two kinks in $H_{c_1}(\phi)$, for $\kappa=50$ and $\epsilon=1/40$. This allows the orientation of the chains state between two forbidden regions.

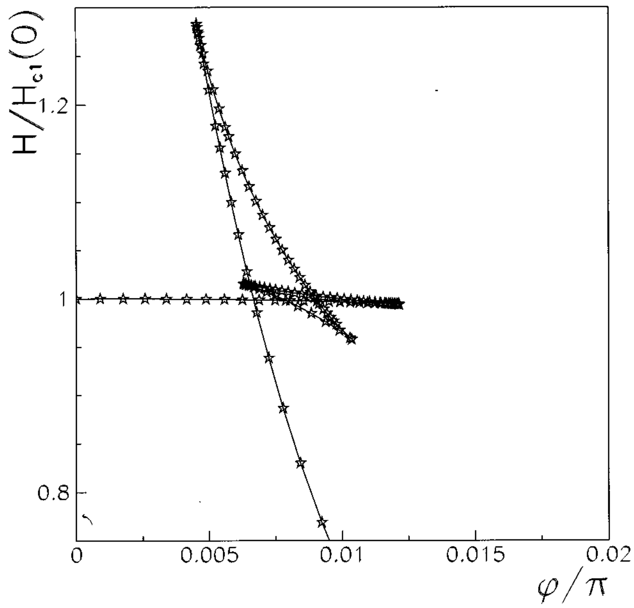

FIG. 16. $\mathcal{H}(\phi)$ for $\kappa=50$ and $1/\epsilon=100$, showing that at large anisotropy the second kink in H_{c_1} disappears.

Due to the anisotropy induced attractive flux-line interaction, the form of the equilibrium flux line lattice has to be determined numerically at all fields. There is a smooth crossover from a large-field Abrikosov-like state to the low-field chainlike state. The nature of the instabilities observed in this equilibrium lattice is complex. At large fields it is stable. As the field is reduced, at a particular field b^* some of the normal modes of the elasticity matrix become unstable. This field depends on the anisotropy ϵ and the angle θ at which the flux lines are orientated to the crystal c axis. The instability is characterized by always having finite k_x and k_z, and we call this a staircase wave instability to distinguish it from a tilt-wave instability which is defined as an instability which depends only on k_z. There is a minimum anisotropy required before these instabilities are observed. This depends on κ and for $\kappa=20$ the instabilities were seen for $1/\epsilon^2>120.3$, but this was increased to $1/\epsilon^2>138$ for $\kappa=50$. This may indicate why the Bitter patterns observed on YBCO are different from those on BSCCO.

As the component of $\mathbf{k}$ along the flux lines is nonzero, the choice of cutoff is crucial. We have used the cutoff suggested by Sudbø and Brandt, where $S(\mathbf{k})=\exp-2g(\mathbf{k})$ and $g(\mathbf{k})=\xi_{ab}^2(\mathbf{k}\times\mathbf{c})^2+\xi_c^2(\mathbf{k}\cdot\mathbf{c})^2$. This cutoff appears more physical than a cutoff that just depends on $\mathbf{k}_\perp$ and allows the elastic instabilities and the nonmonotonic behavior of $\phi(\theta)$ to be related to a single quantity, the line tension $P_l(\theta)$, as expected. However, it should be noted there are still problems associated with this cutoff in the limit $k_z\to\infty$. Once in the region where k_z forces $S(\mathbf{k})\ll 1$, the elasticity matrix (13) will be dominated by $-\Sigma_{\mathbf{Q}} f_{\alpha\beta}(\mathbf{Q})$. While Φ_{xy} is zero, the eigenvalues of the elasticity matrix are negative, showing London theory is always unstable at all fields and angles. However, these instabilities occur at values of $k_z\approx O(1/\xi)$ and are unphysical. The inclusion of core effects, e.g., core bending energy, may remove remove this instability, but this is outside the domain of validity of the London approximation.

Instabilities can also be observed by investigating the lower critical field H_{c_1}, i.e., $b=0$. These $b=0$ instabilities are different from the large field staircase wave instabilities. When the applied field $\mathcal{H}$ is tilted away from the crystal axis, the **B** field and the applied field $\mathcal{H}$ are not parallel. In Sec. V it was seen that for small fields and large anisotropies there existed a nonmonotonic relationship between the angle θ at which the **B** field is tilted away from the c axis, and the angle ϕ at which the applied field is tilted. The nonmonotonicity is related to the elastic instabilities observed, but also imply there is a restriction on the allowed orientations of the **B** field and a kink in $H_{c_1}(\phi)$. The properties of the chain state changes at three different values of the anisotropy. For $1/\epsilon<\Gamma_1$, all possible orientations of the chain state are possible, while in the interval $\Gamma_1<1/\epsilon<\Gamma_2$ the chains cannot be orientated over the range $\theta^*_{2'}<\theta<\theta^*_2$. However, if $\Gamma_2<1/\epsilon<\Gamma_3$ the flux lines are excluded over two separate regions which grow to one large region for $1/\epsilon>\Gamma_3$. This unusual behavior can also be described as $H_{c_1}(\phi)$ developing one kink at $1/\epsilon=\Gamma_1$, a second kink developing at $1/\epsilon=\Gamma_2$ but $H_{c_1}(\phi)$ only having a single kink for $1/\epsilon>\Gamma_3$.

Whether the peculiar effect of having the allowed orientations $\theta^*_{1'}<\theta<\theta^*_{2'}$ between two forbidden regions really exists is unclear. Just as the existence of the forbidden region $\theta^*_1<\theta<\theta^*_2$ for the isolated flux lines in Sec. V may have been an indicator of a state with a lower free energy and applied field H_{c_1}, there may exist a new composition of flux lines that will be stable at large anisotropies and have a lower free energy and applied field H_{c_1} than the chain state. This may be a completely new state or a superposition of chain states and other flux lines, but a full investigation of such states is left for future work.

ACKNOWLEDGMENTS

This work was funded by EPSRC Grant No. GR/J60681.

[1] P.L. Gammel, D.J. Bishop, J.P. Rice, and D.M. Ginsberg, Phys. Rev. Lett. **68**, 3343 (1992).
[2] I.V. Grigorieva, J.W. Steeds, and K. Sasaki, Phys. Rev. B **48**, 16 865 (1993).
[3] C.A. Bolle, P.L. Gammel, D.G. Grier, C.A. Murray, D.J. Bishop, D.B. Mitzi, and A. Kapitulnik, Phys. Rev. Lett. **66**, 112 (1991).
[4] I.V. Grigorieva, J.W. Steeds, G. Balakrishnan, and D.M. Paul, Phys. Rev. B **51**, 3765 (1995).
[5] A.M. Grishin, A.Yu. Martynovich, and S.U. Yampolskii, Sov. Phys. JETP **70**, 1089 (1990).
[6] A.I. Buzdin and A.Yu Simonov, Physica C **168**, 421 (1990).
[7] D.A. Huse, Phys. Rev. **B46**, 12 230 (1992).
[8] A. Sudbø, E.H. Brandt, and D.A. Huse, Phys. Rev. Lett. **71**, 1451 (1993).
[9] A.A. Abrikosov, Sov. Phys. JETP **5**, 1174 (1957).
[10] L.J. Campbell, M.M. Doria, and V.G. Kogan, Phys. Rev. B **38**, 2439 (1988).
[11] K.G. Petzinger and G.A. Warren, Phys. Rev. B **42**, 2023 (1990).
[12] M. Yethiraj, G.D. Wignal, R. Cubitt, E.M. Forgan, S.L. Lee, D.M. Paul, and T. Armstrong, Phys. Rev. Lett. **71**, 3019 (1993).
[13] A. Sudbø and E.H. Brandt, Phys. Rev. Lett. **68**, 1758 (1992).
[14] E. Sardella and M.A. Moore, Phys. Rev. B **48**, 9664 (1993).
[15] A.K. Nguyen and A. Sudbø, Phys. Rev. B **53**, 834 (1996).
[16] G. Blatter, V.B. Geshkenbein, and A.I. Larkin, Phys. Rev. Lett. **68**, 875 (1992).
[17] L.L. Daemen, L.J. Campbell, and V.G. Kogan, Phys. Rev. B **46**, 3631 (1992).
[18] E. Sardella, Phys. Rev. B **53**, 14 506 (1996).
[19] E.H. Brandt, J. Low Temp. Phys. **26**, 735 (1977).
[20] W. Barford and J.M.F. Gunn, Physica C **156**, 515 (1988).
[21] E.H. Brandt, Rep. Prog. Phys. **58**, 1465 (1995).
[22] R.A. Klemm, Phys. Rev. B **47**, 14 630 (1993).
[23] E.M. Forgan and S.L. Lee, Phys. Rev. Lett. **75**, 1422 (1995).
[24] L.J. Campbell, M.M. Doria, and V.G. Kogan, Phys. Rev. B **38**, 2439 (1988).
[25] W.H. Press, S.A. Teukolsky, W.T. Vetterling, and B.P. Flannery, *Numerical Recipes in Fortran* (Cambridge University Press, Cambridge, U.K., 1986), Chap. 10; R.P. Brent, *Algorithms for Minimization without Derivatives* (Prentice-Hall, Englewood Cliffs, New Jersey, 1973), Chap. 5.
[26] A. Sudbø and E.H. Brandt, Phys. Rev. B **43**, 10 482 (1991).
[27] E. Sardella, Phys. Rev. B **45**, 3141 (1992).
[28] A. Sudbø and E.H. Brandt, Phys. Rev. Lett. **66**, 1781 (1991).